

East Asian aerosol cleanup has likely contributed to the recent acceleration in global warming

Article

Published Version

Creative Commons: Attribution 4.0 (CC-BY)

Open Access

Samset, B. H. ORCID: <https://orcid.org/0000-0001-8013-1833>, Wilcox, L. J. ORCID: <https://orcid.org/0000-0001-5691-1493>, Allen, R. J. ORCID: <https://orcid.org/0000-0003-1616-9719>, Stjern, C. W. ORCID: <https://orcid.org/0000-0003-3608-9468>, Lund, M. T. ORCID: <https://orcid.org/0000-0001-9911-4160>, Ahmadi, S. ORCID: <https://orcid.org/0000-0002-2754-4820>, Ekman, A., Elling, M. T., Fraser-Leach, L. ORCID: <https://orcid.org/0009-0003-9452-5528>, Griffiths, P., Keeble, J., Koshiro, T. ORCID: <https://orcid.org/0000-0003-2971-7446>, Kushner, P. ORCID: <https://orcid.org/0000-0002-6404-4518>, Lewinschal, A., Makkonen, R. ORCID: <https://orcid.org/0000-0002-8961-3393>, Merikanto, J., Nabat, P. ORCID: <https://orcid.org/0000-0001-7034-638X>, Narazenko, L., O'Donnell, D. ORCID: <https://orcid.org/0000-0002-2700-471X>, Oshima, N. ORCID: <https://orcid.org/0000-0002-8451-2411>, Rumbold, S. T. ORCID: <https://orcid.org/0000-0001-8138-4541>, Takemura, T. ORCID: <https://orcid.org/0000-0002-2859-6067>, Tsigaridis, K. ORCID: <https://orcid.org/0000-0001-5328-819X> and Westervelt, D. M. ORCID: <https://orcid.org/0000-0003-0806-9961> (2025) East Asian aerosol cleanup has likely contributed to the recent acceleration in global warming.

Communications Earth & Environment, 6 (1). 543. ISSN 2662-4435 doi: 10.1038/s43247-025-02527-3 Available at <https://centaur.reading.ac.uk/123626/>

It is advisable to refer to the publisher's version if you intend to cite from the work. See [Guidance on citing](#).

Published version at: <https://doi.org/10.1038/s43247-025-02527-3>

To link to this article DOI: <http://dx.doi.org/10.1038/s43247-025-02527-3>

Publisher: Springer Nature

All outputs in CentAUR are protected by Intellectual Property Rights law, including copyright law. Copyright and IPR is retained by the creators or other copyright holders. Terms and conditions for use of this material are defined in the [End User Agreement](#).

www.reading.ac.uk/centaur

CentAUR

Central Archive at the University of Reading

Reading's research outputs online

<https://doi.org/10.1038/s43247-025-02527-3>

East Asian aerosol cleanup has likely contributed to the recent acceleration in global warming



Bjørn H. Samset¹✉, Laura J. Wilcox², Robert J. Allen³, Camilla W. Stjern¹, Marianne T. Lund¹, Sharar Ahmadi², Annica Ekman⁴, Maxwell T. Elling^{5,6}, Luke Fraser-Leach⁷, Paul Griffiths⁸, James Keeble⁹, Tsuyoshi Koshiro¹⁰, Paul Kushner⁷, Anna Lewinschal⁴, Risto Makkonen¹¹, Joonas Merikanto¹¹, Pierre Nabat¹², Larissa Narazenko^{13,14}, Declan O'Donnell¹¹, Naga Oshima¹⁵, Steven T. Rumbold², Toshihiko Takemura¹⁵, Kostas Tsigaridis^{13,14} & Daniel M. Westervelt^{14,16}

Global surface warming has accelerated since around 2010, relative to the preceding half century^{1–3}. This has coincided with East Asian efforts to reduce air pollution through restricted atmospheric aerosol and precursor emissions^{4,5}. A direct link between the two has, however, not yet been established. Here we show, using a large set of simulations from eight Earth System Models, how a time-evolving 75% reduction in East Asian sulfate emissions partially unmasks greenhouse gas-driven warming and influences the spatial pattern of surface temperature change. We find a rapidly evolving global, annual mean warming of 0.07 ± 0.05 °C, sufficient to be a main driver of the uptick in global warming rate since 2010. We also find North-Pacific warming and a top-of-atmosphere radiative imbalance that are qualitatively consistent with recent observations. East Asian aerosol cleanup is thus likely a key contributor to recent global warming acceleration and to Pacific warming trends.

Over the industrial era, anthropogenic emissions of atmospheric aerosols, and their gaseous precursors, have strongly influenced the Earth's climate and energy balance⁶. Aerosols have recently been assessed to have cooled the global surface by 0.4 °C (the year 2019, relative to pre-industrial conditions), partially masking greenhouse gas-driven warming, predominantly through aerosol–cloud interactions affecting the albedo and coverage of clouds, alongside direct aerosol shortwave effects⁷. The geographical distribution of this forcing has, however, shifted after 1980, with China and India having replaced the US and Europe as the major emitters⁸. It has shifted again since the early 2010s, following China's strong effort to reduce air pollution, which has led to strong (~20 Tg/year, or around 75%) sustained reductions in the emission rate of SO₂^{4,9}, the precursor gas of sulfate aerosols, which in turn is the dominating aerosol species currently cooling the Earth⁷.

Concurrently, the rate of global mean surface warming, which has overall been constant at around 0.18 °C/decade since around 1970, has increased^{1,2}. Recent studies find an acceleration in the rate of surface warming and ocean heat uptake after 1990, and the most recent decade (2013–2022) had a warming rate of 0.25 °C/decade, even after reducing the influence of internal variability^{1,3}. 2023 and 2024 were both record-setting in terms of surface temperature anomaly, dominated by strong positive sea-surface temperature anomalies in most ocean basins¹⁰.

Recent improvements in satellite-based constraints on the Earth's Radiative Imbalance at top-of-atmosphere (TOA) have also revealed increased energy absorption into the global Earth system¹¹. A range of studies have suggested that aerosol emissions changes may have been contributing factors. These include recent overall trends in global aerosol

¹CICERO Center for International Climate Research, Oslo, Norway. ²National Centre for Atmospheric Science, University of Reading, Reading, UK. ³Department of Earth and Planetary Sciences, University of California Riverside, Riverside, CA, USA. ⁴Department of Meteorology, Bolin Centre for Climate Research, Stockholm University, Stockholm, Sweden. ⁵Department of Atmospheric and Oceanic Sciences, University of Colorado Boulder, Boulder, CO, USA. ⁶Cooperative Institute for Research in Environmental Sciences, University of Colorado Boulder, Boulder, CO, USA. ⁷Department of Physics, University of Toronto, Toronto, ON, Canada. ⁸School of Chemistry, University of Bristol, Bristol, UK. ⁹Lancaster Environment Centre, Lancaster University, Lancaster, UK. ¹⁰Meteorological Research Institute, Japan Meteorological Agency, Ibaraki, Japan. ¹¹Finnish Meteorological Institute, Helsinki, Finland. ¹²Centre National de Recherches Météorologiques, Toulouse, France. ¹³NASA Goddard Institute of Space Studies, New York, NY, USA. ¹⁴Lamont-Doherty Earth Observatory, Columbia Climate School, New York, NY, USA. ¹⁵Research Institute for Applied Mechanics, Kyushu University, Fukuoka, Japan. ¹⁶Center for Climate Systems Research, Columbia University, New York, NY, USA. ✉e-mail: b.h.samset@cicero.oslo.no

loading¹², and the regulations by the International Maritime Organization that caused a strong drop in SO₂ emissions from the global shipping fleet from 2020 and onwards^{13,14}. Low planetary albedo due to reduced cloud amounts, or cloud albedo, in the North Pacific was also recently implicated as a related process leading to increased surface warming, albeit for a single year (2023)¹⁵.

However, few studies have to date quantified the influence of the recent emissions reductions in East Asia on global and regional climate evolution, despite their being larger in magnitude than the shipping emission changes, and sustained for longer (~9 Tg/year since 2020¹³). Such analysis requires dedicated simulations with Earth System Models that have not been readily available, partly due to a lack of updated emissions inventories that capture the decrease in, primarily, emissions from mainland China. Zheng et al.⁵ estimated a mean Northern Hemisphere warming of 0.12 ± 0.01 °C, but using a single CMIP5 era model (CESM 1.2.2) and idealized equilibrium simulations. The regional nature of the emissions change also means that internal variability is a major limiting factor in quantifying a climate response, necessitating multiple ensemble realizations of these simulations. Recent global modeling exercises such as CMIP6 used global emissions changes¹⁶, where the influence of East Asian SO₂ emissions cannot be separated from other, concurrent changes. Further, the emissions dataset used in CMIP6 did not accurately represent the recent reduction in East Asian aerosol precursors¹⁷, with marked consequences for regional climate evolution as reported by Wang et al.¹⁸. Yet other studies have investigated teleconnections from East Asian emissions onto sea-surface warming patterns in the North Pacific, but did not connect these to global surface temperature evolution^{19,20}.

Here, we present results from the Regional Aerosol Model Inter-comparison Project (RAMIP), where aerosol emissions were systematically perturbed in individual source regions, in eight CMIP6 era Earth System Models²¹. We show results from a transient emissions reduction experiment in an East Asia region, consisting primarily, but not solely, of mainland

China, that are closely analogous to recent emissions changes. RAMIP simulations span 2015–2049, and for the latter 15-year period (2035–2049) they have an East Asian SO₂ emission reduction of 20 Tg/year, i.e., comparable to that which occurred in the real world since around 2010. Thus, we can use the RAMIP simulations for this period to quantify the real-world climate impacts of recent efforts by China to improve air quality, including surface temperatures, precipitation, and the global energy imbalance. By comparing observations of regional temperature changes and the TOA radiation imbalance, we argue that the recent aerosol emissions changes in East Asia are a key contributing factor, among others, to the recent uptick in the rate of global mean surface warming, through an unmasking of greenhouse gas-driven climate change.

Results

RAMIP simulations and recent emissions changes in East Asia

We first document the emissions perturbation applied in the RAMIP *baseline* and *East Asia* simulations²¹ (see “Methods”), and compare them to the actual emissions reductions from the same region since around 2010. Briefly, RAMIP isolates the climate effects of aerosol emissions in one region by comparing two sets of transient emission simulations; one following a global, high emissions pathway (SSP3-7.0, which assumes weak air quality policies), and one where aerosol emissions in one region (*East Asia*, consisting mainly of mainland China emissions) have been replaced by those from a strong air quality policy trajectory (SSP1-2.6). See “Methods,” or²¹, for a full description. In the present analysis, we use simulations from 8 global models, each with 10 ensemble members, for a total of 80 ensemble members. This simulation set effectively samples both model uncertainty and internal climate variability.

Figure 1a shows changes in aerosol optical depth (AOD) retrieved by MODIS Terra and Aqua between the two previous decades. Consistent with previous literature, we find a dipole pattern consisting of an increase over India and a strong decrease over China following their air quality

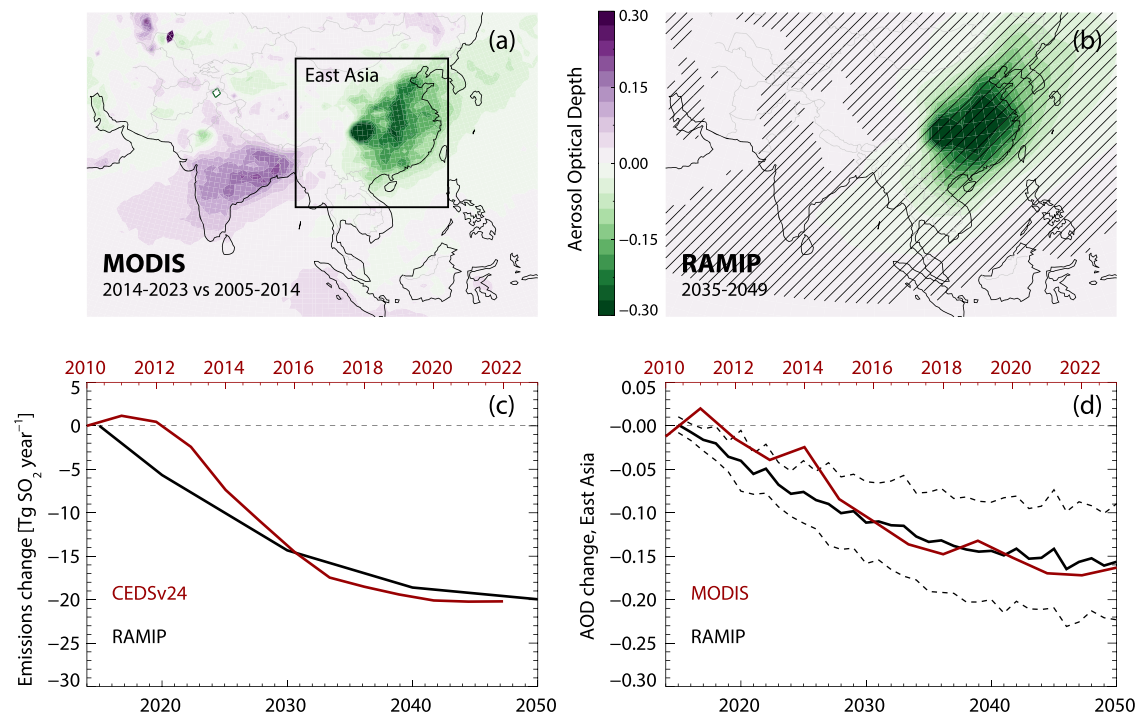


Fig. 1 | Observed changes in aerosol optical depth since 2010, and the corresponding changes in emissions and in the RAMIP model simulations. a AOD observations, difference between 2014–2023 and 2005–2014. Mean of MODIS Aqua and Terra. The Inset box shows the East Asia domain used throughout this paper. **b** Spatial distribution of AOD change in RAMIP. Multi-model (80 ensemble member) mean, difference between the East Asia and Baseline simulations. Hatching

indicates statistical significance (see “Methods”). **c** Annual SO₂ emissions difference, relative to 2010, in CEDSv2024 (red), and between the two scenarios used by RAMIP (black). Mean over the East Asia domain. **d** AOD change, mean over the East Asia domain, from MODIS (red) and in RAMIP (black). The range is ± 1 standard deviation of the RAMIP multi-model response.

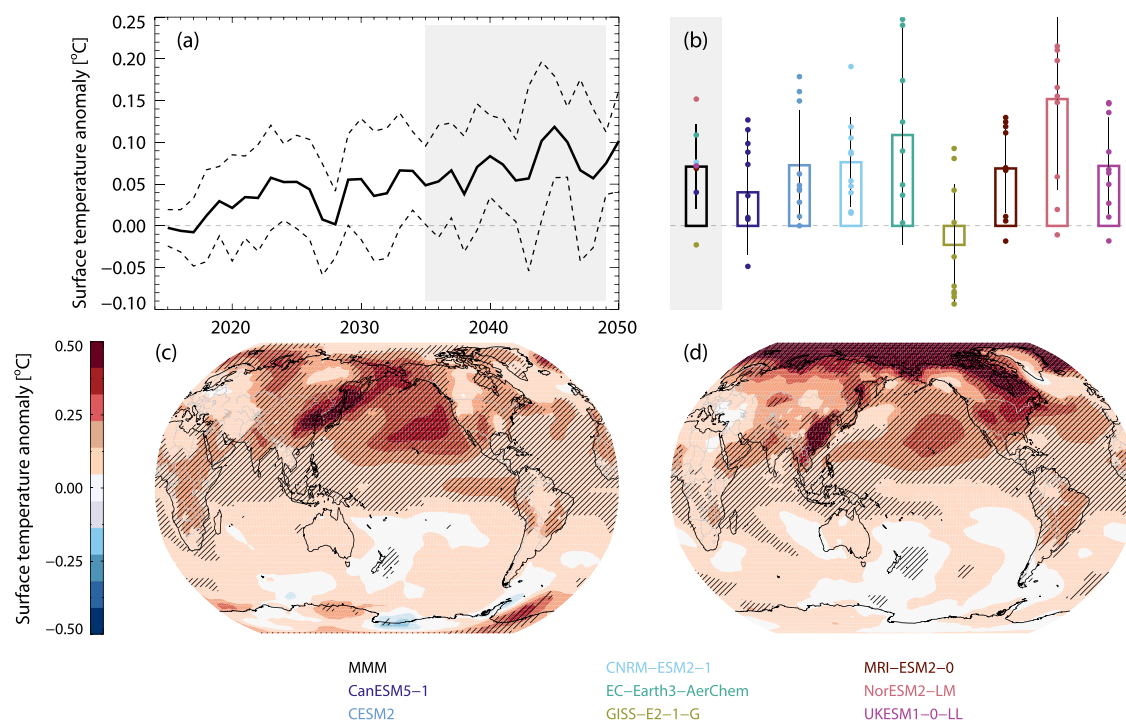


Fig. 2 | Surface temperature responses to reductions in East Asian aerosol emissions. **a** Global, annual mean surface temperature response to the RAMIP East Asian aerosol emissions perturbations, multi-model mean (MMM) and ± 1 standard deviation range. **b** Ensemble member, model mean, and multi-model mean

temperature response for 2035–2049. Vertical lines show ± 1 standard deviation. Y axis is as for (a). **c** Multi-model spatial response, for June–July–August. **d** As (c), for December–January–February.

improvement initiatives. For comparison, Fig. 1b shows the pattern of AOD change between the RAMIP *East Asia* and *baseline* simulations, for the simulated period 2035–2049. Here, and elsewhere, this time period is chosen for RAMIP to sample the climate response after most of the emission reductions have occurred, while maximizing the number of years (RAMIP simulations end in 2050, so 2049 is the last year we can use while also letting the last DJF season run into the following year.) Fig. 1c, d shows the corresponding SO_2 emissions and AOD change, for observations and simulations, within the box labeled East Asia in Fig. 1a (a geographical box that covers the main emission regions).

For observations, relative to the 2005–2010 period, we find an AOD change of -0.13 units for the period 2014–2023, resulting primarily from emissions reductions of around $20 \text{ Tg SO}_2/\text{year}$ (Supplementary Fig. 1b). The emissions data are from the December 2024 release of the Community Emissions Data System (CEDS)²², which includes updated estimates of recent East Asian SO_2 emission changes. Concurrent changes in black carbon aerosol emissions are shown in Supplementary Fig. 1; they are smaller, in absolute terms and in particle number, and are not expected to contribute strongly to the AOD change, though they may influence climate features through their strong atmospheric shortwave absorption²³.

RAMIP transient simulations start in 2015 but use CMIP6 emissions based on a CEDS version that projected a delayed reduction in East Asia emissions compared to the actual, realized changes. The RAMIP *East Asia* and *baseline* simulations, however, still have an emissions difference trajectory that broadly corresponds to recent observations ($20 \text{ Tg SO}_2/\text{year}$), for the last 15 years of the RAMIP simulations (2035–2049). In the following, we use this period to quantify RAMIP climate responses (see “Methods”). We also find a multi-model mean AOD change trajectory and magnitude that broadly tracks MODIS observations (ΔAOD of -0.11 ± 0.05 units for the RAMIP period 2035–2049). We do note, however, that even though all models used the same emissions, the RAMIP 2035–2049 mean East Asia AOD change ranges from -0.08 to -0.28 , and the local magnitudes do differ from MODIS observations (see Fig. S1). This

is due to a combination of factors including the optical properties of the simulated aerosols, the cloud fields, wind and precipitation climatologies, and aerosol removal rates. See further discussion on model diversity below.

Physically, AOD decreases are associated with less scattering of incoming solar radiation and hence increases in downwelling surface solar radiation. Supplementary Fig. 1 shows the corresponding changes in downwelling shortwave radiation at the surface, in response to aerosol emissions reductions. Here, we find a multi-model mean change of $7.7 \pm 2.5 \text{ W m}^{-2}$, over the East Asia domain, with inter-model variation and spatial pattern that broadly follow that of AOD.

Based on Fig. 1 and Supplementary Fig. 1, we conclude that the RAMIP East Asia results for the 2035–2049 period can be used as a proxy for the response to the emission rate change that has occurred in the real world over the 2010–2023 period (i.e., a 20 Tg/year sustained reduction in SO_2 emissions). We note that neither the overall conclusions nor the absolute numbers cited below are sensitive to changing the endpoints of these time periods by up to 2 years.

Modeled temperature and precipitation changes

In the RAMIP simulations, we find robust changes in both temperature and precipitation in response to East Asian aerosol emission reductions, with a mean change that extends beyond the interannual variability in the multi-model, multi-ensemble-member mean. In Fig. 2, we show the global, annual mean temperature responses to a 20 Tg/year reduction in SO_2 emissions from East Asia. For 2035–2049, we find a multi-model mean global warming of $0.07 \pm 0.05 \text{ }^\circ\text{C}$, where the uncertainty is the standard deviation of the eight individual model results. The signal evolves in overall correspondence with the emission reductions, indicating a rapid climate response to SO_2 emissions reductions, in line with previous studies²⁴. The overall rate of change for the full 2015–2049 period is $0.02 \text{ }^\circ\text{C/decade}$. Note also the strong inter-model variability (Fig. 2b), with one model (NorESM2-LM) showing an ensemble mean warming of $0.15 \text{ }^\circ\text{C}$, while another outlier (GISS-E2-1-G) even shows a slight cooling ($-0.02 \text{ }^\circ\text{C}$). We link these model

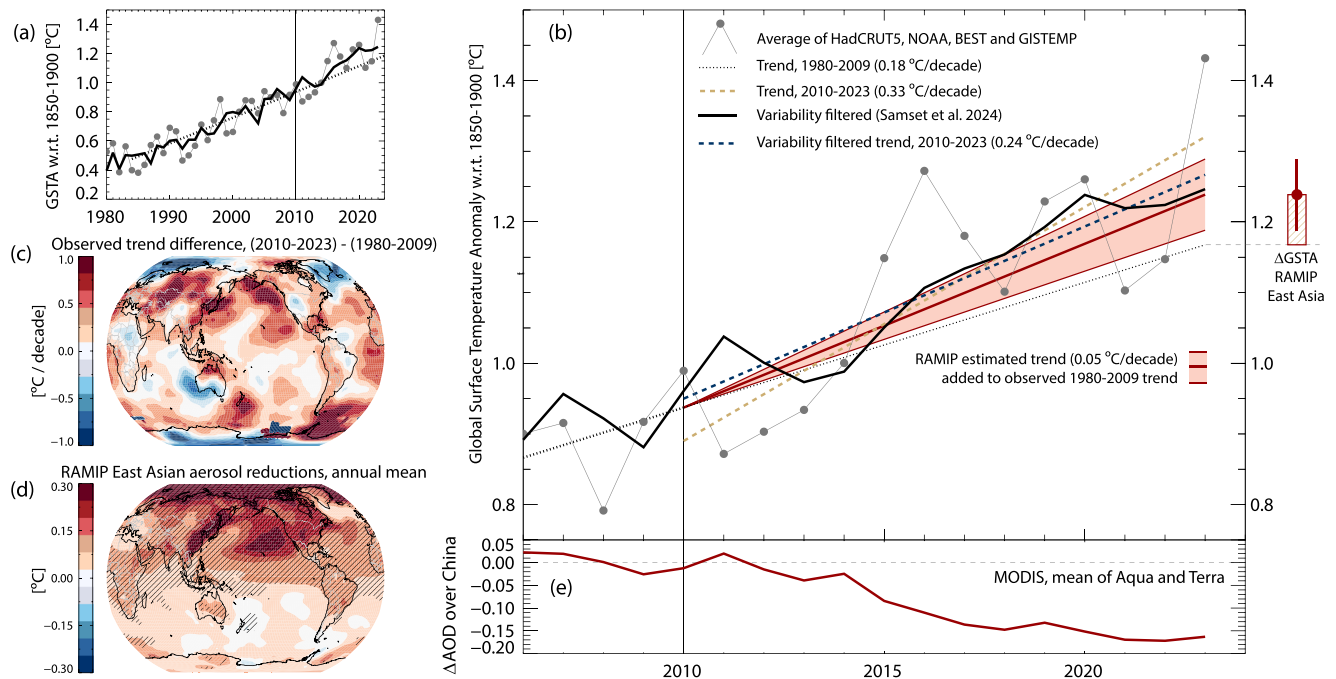


Fig. 3 | Warming from reductions in East Asian aerosol emissions in the context of recent surface temperature changes. **a** Global Surface Temperature Anomaly (GSTA) relative to 1850–1900, mean of four data series (HadCRUT5, NOAA, BEST, GISTEMP). The black line shows a derived dataset where interannual variability has been filtered out based on oceanic modes of variability (Samset et al.¹⁰). Dashed line: 1980–2010 linear trend, extended through 2023. **b** As (a), with added trend lines for

2010–2023. The red line and range, and right-hand box, show the RAMIP estimate of warming due to East Asian aerosol emissions reductions, added to the extension of the observed 1980–2010 linear trend. **c** Regional differences in 1980–2010 and 2010–2023 trends. Mean of the four data series. **d** RAMIP spatial annual mean surface temperature response to East Asian aerosol emission reductions. **e** AOD change from MODIS, as Fig. 1a.

differences, in particular the outlier models, primarily to aerosol–cloud interactions in the North Pacific, and to Arctic amplification that is known to be strong both for Asian aerosol emissions, and for our warmest model (NorESM2-LM)²⁵. See also Supplementary Fig. 2, and further discussion on the radiative responses of the models below.

There is also a strong contribution from internal variability, with marked diversity between ensemble members (Fig. 2b). This is partly due to our compromise usage of a 15-year time period to quantify a climate response, where internal variability will contribute strongly, and partly due to the overall forcing strength, again relative to internal variability. This illustrates the difficulties of quantifying the climate impacts of the recent East Asian aerosol emission reductions, and other notable emissions changes like those resulting from the recent IMO shipping regulations²⁶ and the importance of conducting large ensemble simulations when investigating climate forcings that are strong regionally but weaker on a global scale²¹.

Geographically, the seasonal temperature change is strongest ($\sim 1^\circ\text{C}$) near the source (East Asia, notably Eastern and Northern China) both in boreal summer (JJA, Fig. 2c) and winter (DJF, Fig. 2d). However, we also find significant warming ($>0.2^\circ\text{C}$; paired Student's *t*-test, $p < 0.05$) over much of the North Pacific, in both seasons. For DJF, we also find a significant warming of North America, and throughout the Arctic. This is in line with previous studies that have found a strong long-range contribution to arctic amplification from Asian aerosol emissions^{27,28}. A wintertime cooling patch in Central Europe that has been reported by previous studies^{29,30} is however not visible in our dataset. For annual and seasonal mean responses, including for individual models and ensemble members, see Supplementary Figs. 2–4.

Supplementary Fig. 5 shows the corresponding precipitation response, which broadly tracks that of surface temperature. We find an overall global wettening of 0.009 ± 0.004 mm/day ($0.3 \pm 0.1\%$), yielding an overall hydrological sensitivity of $4 \pm 2\%^\circ\text{C}$, which is broadly consistent with previous estimates of the climate impacts of aerosol emissions changes³¹.

Geographically, we find a strong summertime (JJA) precipitation increase in East China, and along the East Asian coastline, as well as a wettening along the North Pacific storm tracks extending well into North America. We also find a northward shift of the ITCZ, consistent with expectations from preferential warming of the Northern Hemisphere relative to the Southern Hemisphere³². The regions with statistical significance are smaller than for temperature, as expected due to the higher internal variability and greater model diversity in precipitation simulations.

Influence on recent global warming and radiative imbalance

We now put the RAMIP results in the context of recent trends in global warming, in Fig. 3. In Fig. 3a, we show the global mean surface temperature anomaly (GSTA) relative to 1850–1900 since 1980, as the average of four observational reconstructions (HadCRUT5, NOAA, GISTEMP and Berkeley Earth; see “Methods”). For the 30-year period of 1980–2009, used for consistency with previous literature on the multi-decadal rate of surface warming³, the average observed warming rate is $0.18 \pm 0.02^\circ\text{C}/\text{decade}$. For illustration, we also show the time series from ref. 10, where internal variability from Pacific ENSO and other ocean modes of variability has been filtered out (our conclusions do not rely on the usage of this dataset). For the subsequent period of 2010–2023, we find an elevated observed warming rate of $0.33 \pm 0.17^\circ\text{C}/\text{decade}$, and $0.25 \pm 0.06^\circ\text{C}/\text{decade}$ when interannual variability is filtered, consistent with previous studies^{2,3}. Note that uncertainties in this section are 95% confidence intervals on the linear regressions.

In the main panel (Fig. 3b), we zoom in on the latter period. Most post-2010 GSTA values fall above the continuation of the 1980–2009 trend (dotted black line), in the reconstructions (dots) and in the reduced variability time series (solid black line), indicating a recent increase in the global warming rate. To estimate the contribution of East Asian aerosol emissions changes to this increase, we take the RAMIP quantified global warming of $0.07 \pm 0.05^\circ\text{C}$, and convert it to a warming rate over the 2010–2023 period ($0.05 \pm 0.04^\circ\text{C}/\text{decade}$). See the box-and-whisker on the right of Fig. 3b,

which shows how we've added this aerosol cleanup-induced warming rate (red line and range) to the continuation of the 1980–2009 trend.

Assuming, for now, no change in the underlying greenhouse gas-induced global warming rate, this suggests a combined post-2010 warming rate, from greenhouse gas increases and East Asian aerosol cleanup, of $0.18\text{ }^{\circ}\text{C/decade} + 0.05\text{ }^{\circ}\text{C/decade} = 0.23\text{ }^{\circ}\text{C/decade}$, approaching the $0.25\text{ }^{\circ}\text{C/decade}$ found after filtering the effects of internal variability. Note that prior to 2010, increases in East and South Asian aerosol emissions were broadly compensated for by reductions in Europe and the US, leading to an overall geographical shift in aerosol loadings³³. For further context, see the discussion below of other sources of recent warming.

Note also that we assume here that the full warming due to the observed recent East Asian emissions reduction has already been realized, so that it is justifiable to compare warming in observations during the 2010–2023 period to warming in the RAMIP simulations during the 2035–2049 period. This is supported by recent modeling exercises using sustained step changes in SO_2 emissions³⁴, finding that the majority of subsequent global mean surface temperature change has been realized within the first 24 months, while the rest develops slowly at a multi-decadal timescale. The transient RAMIP simulations also do not show any appreciable delay in the climate response to SO_2 reductions. However, our estimate should still be taken as an upper limit, to take this limitation into account.

Since aerosol changes have regionally heterogeneous climate influences, as shown above, we next investigate the correspondence of simulated changes to observed regional warming rate. In Fig. 3c, we show the observed difference between the 2010–2023 and 1980–2009 warming rates in the four reconstructions. See Supplementary Fig. 6 for individual time series and the two trend periods in isolation. In Fig. 3d, we show the annual mean surface warming pattern from East Asian aerosol emission reductions in RAMIP. In both cases, we find a pattern of observed warming in the North Pacific, with two distinct maxima: one along the East Asian coastline, and the other following the west coast of North America, extending west to the center of the Pacific. This shows that the simulated increased global mean warming rate comes from a geographical region where observations also find an elevated warming rate since 2010, relative to previous decades. See Supplementary Fig. 10 for the transient evolution of regional means (Western and Eastern North Pacific) for individual models. An important caveat, however, is that for the observations, a 13-year trend will be strongly influenced by decadal scale variability, notably the Pacific Decadal Oscillation (PDO), which has changed markedly over the time period studied here³⁴.

Top-of-atmosphere radiative imbalance

While the influence of oceanic modes of variability is beyond the scope of the present study, we can relate our results to recent discussions of aerosol influences on the change in TOA energy imbalance. In Fig. 4, we investigate the TOA all-sky change in radiative imbalance (shortwave plus longwave) in response to East Asian aerosol emissions reductions in RAMIP, and compare them to observations (CERES) and reanalysis (ERA5). Figure 4a, b shows the time series and 2035–2049 means of the TOA all-sky radiative imbalance, which has a mean of $0.06 \pm 0.04\text{ Wm}^{-2}$. While there is substantial inter-model and ensemble member variability, the overall evolution is very similar between the eight RAMIP models. Using the same logic as above, this corresponds to an evolving increase in the TOA imbalance since 2010 of $0.05 \pm 0.03\text{ Wm}^{-2}/\text{decade}$.

Figure 4c, d shows the geographical distributions of clear sky and all-sky radiative imbalances. Again, for all-sky conditions, we find a geographical pattern displaying two clear maxima, near the source region, and in the western North Pacific, with peak values exceeding 2 Wm^{-2} . There is little influence on other regions. For clear sky conditions, only the East Asian and eastern North Pacific influence remains, indicating it has a major contribution from the direct interaction of aerosols with incoming sunlight. The maximum west of North America, however, is likely primarily a result of aerosol–cloud interactions, seen in a region with a high prevalence of low clouds (stratocumulus decks). Supplementary Fig. 7 shows individual

models, while Supplementary Fig. 10 shows a further breakdown into shortwave and longwave components.

This result also explains part of the inter-model diversity in RAMIP responses. See Supplementary Fig. 9, which shows the annual mean cloud climatologies of the models. The models that have low overall temperature response to East Asian aerosol changes, notably CNRM-ESM2-1 and GISS-E2-1-G, have relatively low cloud fractions in this region, and also very weak radiative responses. The opposite is true for strongly responding models, including CESM2, NorESM2, EC-Earth3-AerChem, and UKESM1-0-LL. The correspondence is not exact, but still indicative that aerosol–cloud interactions in the eastern North Pacific stratocumulus region are a key lever for climate responses to East Asian aerosol emissions. Supplementary Fig. 10 also shows the transient evolution of Western and Eastern North Pacific means of temperature and surface shortwave fluxes. We further note that for clear sky conditions, there is a strong positive anomaly over Eastern China in most models. This indicates the presence of compensating aerosol–cloud effects, and perhaps other aerosol processes such as wet removal by precipitation, over this region in the RAMIP models.

Finally, in Fig. 4e, f, we show recent all-sky TOA imbalance trends from observations (CERES), and its difference from a reanalysis product (ERA5). While the CERES observations (Fig. 4e) have a strong influence on internal variability and will also be influenced by other recent changes in the climate system, we do find a positive anomaly in the North Pacific. The ERA5 reanalysis itself shows a very similar pattern (Supplementary Fig. 5).

ERA5 does include treatment of aerosols, but it uses a CMIP5 era combination of historical emissions up to 2009 and subsequently the RCP emissions³⁵. These pathways do not include the recent reductions in East Asian emissions. Hence, the difference between CERES and ERA5 may be indicative of regions where the recent aerosol changes are important for the reconstruction, and have an influence on observed rates of change of TOA radiative fluxes. To see whether we can see any indication of this, we show the difference between CERES and ERA5 in Fig. 4f. Among the many features that stand out here, we find a positive anomaly in the low cloud region of the eastern North Pacific, as well as a negative anomaly over Eastern China. We note that these are regions where downwind effects of East Asian aerosol emissions would be expected to contribute and that this is indeed where RAMIP simulations indicate an influence from aerosol–cloud interactions. Recall, however, the previous caveat that PDO also changes in the time periods studied here and that trends in sea-surface temperatures will also influence ERA5 reconstructions. This means that we cannot make a clear attribution of the observed changes to aerosol emissions changes with this method, but rather point this out as an area for further, more in-depth studies.

Other sources of recent warming

We have shown how recent aerosol emissions reductions in East Asia likely had a strong influence on post-2010 elevated rates of surface warming, both globally and in the North Pacific. To put these results in context, we here discuss some other, concurrent changes that we cannot consider in the same framework.

One anthropogenic factor is the accelerated increase in atmospheric CH_4 concentrations over the same period. As an estimate, using recent global near-surface concentrations from NOAA³⁶ and the IPCC AR6³⁷, combined with the forcing estimation methods from ref. 38, we find a global mean CH_4 radiative forcing (RF) of 0.06 Wm^{-2} for the 2010–2023 period, corresponding to a rate of $0.047\text{ Wm}^{-2}/\text{decade}$. This is a marked increase over the previous decade (2000–2010), where we find $0.01\text{ Wm}^{-2}/\text{decade}$. However, for the full 30-year period of 1980–2010, we estimate a forcing of $0.043\text{ Wm}^{-2}/\text{decade}$. This means that while changes in CH_4 atmospheric concentration growth rates may have contributed to decadal variability, and clearly can enhance the overall rate of global warming, the recent decade has not seen a markedly strong influence from CH_4 increases compared to recent history. We also note that the above numbers are for RF, while the Effective Radiative Forcing (ERF), and the temperature influences of methane, may be muted due to rapid adjustments³⁹.

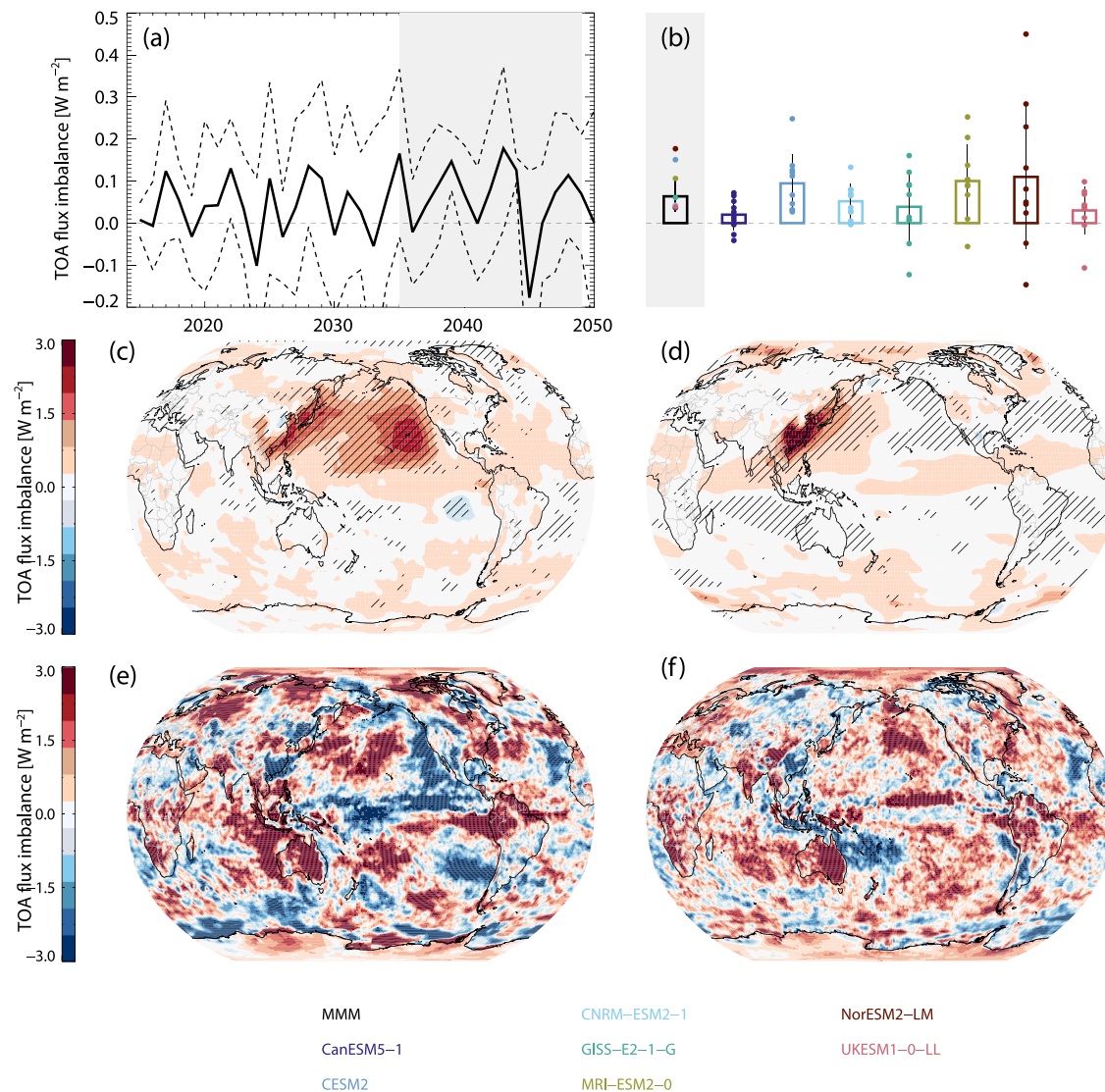


Fig. 4 | Influence of East Asian aerosol emissions reductions on top-of-atmosphere radiative imbalance. **a** Global, annual mean response of the top-of-atmosphere (TOA) radiative flux imbalance to the RAMIP East Asian aerosol emissions perturbations. Multi-model mean (MMM) and ± 1 standard deviation range. **b** Ensemble member, model mean, and multi-model mean TOA imbalance response for 2035–2049. Vertical lines show ± 1 standard deviation. **c** Spatial

distribution of TOA imbalance response, all-sky, for 2035–2049. **d** As (c), for clear sky conditions. **e** TOA imbalance from CERES observations for recent decades (2001–2010 vs 2014–2023, chosen to cover full decades while also maximizing the influence of East Asian aerosol emission reductions). **f** Difference between (e) and the ERA5 reanalysis TOA imbalance for the same time periods.

Another, more recent, anthropogenic factor is the post-2020 reduction in SO_2 emissions from the shipping sector, following the recent regulations of the International Maritime Organization. Here, a range of studies have concluded that the global mean ERF from the 80% reduction in emissions, corresponding to around 9 Tg SO_2 /year, is in the range of 0.05 – 0.10 W m^{-2} ^{26,40,41}. While studies using ensembles of simulations from fully coupled models do find a surface temperature response to these emissions change over time, the magnitude and detectability relative to internal variability for the years 2020–2023 is still disputed^{26,40}. Coming in at the end of the time period studied here, the IMO regulations are unlikely to have had a major influence on the above conclusions regarding the influence of Chinese aerosol emission changes.

ERF estimates are unfortunately not available from all RAMIP models. For those that have delivered the required simulations (see “Methods”), we find an ERF from the emissions changes in East Asia discussed above ranging from 0.06 to 0.21 W m^{-2} ²¹.

Recently, in the context of the 2023 record global mean surface temperatures, Goessling et al.¹⁵ identified a record-low planetary albedo

as a contributing cause. Using the same datasets as here (CERES and ERA5), they highlight low cloud cover over the North Pacific as a key component of this and note that the role of aerosols in this change is still unclear. Their results are well in line with the present study, both geographically and in terms of physical processes; however, their main focus is on reduced cloud fraction in selected years, while our results concern a reduced climate cooling through weaker aerosol impacts on clouds on a decadal scale. The regional similarity, however, opens the possibility that the results of Goessling et al. are, at least in part, interpretable as a sustained reduction in climate cooling through aerosol–cloud interactions.

Discussion

Using a set of 10-ensemble-member simulations from eight CMIP6 era Earth System Models, we have quantified the transient climate response to gradually reduce aerosol emissions from East Asia. We find a global, annual mean warming of $0.07 \pm 0.05^\circ\text{C}$, and a corresponding wettening of around $4 \pm 2\%$ /°C.

The emission reductions in our simulations correspond closely to the emissions reductions realized in East Asia over the period 2010–2023, in magnitude and geographical location. This allows us to put our results in the context of the recent uptick in the observed rate of global mean surface warming. Here, we find that emissions reductions in East Asia have contributed up to 0.05 °C/decade since 2010, explaining a large fraction of the observed increase of 0.06 °C/decade over the same period, after filtering out the effects of interannual variability.

We also find that the geographical location of the temperature influence of a reduction in East Asian SO₂ emissions corresponds to where observations show a recent surge in warming, and also where satellite observations find an increase in TOA radiative imbalance. This lends support to the conclusion that the recent intensive effort to tackle air pollution in China has driven, as an unintended side effect, an unmasking of greenhouse gas-driven global warming and a marked contribution to the recently observed warming trend.

Looking ahead, emissions from East Asia are projected to keep going down. However, the rate of change has slowed markedly, and the CEDS inventory estimates that there is less than 10 Tg SO₂/year (~25% of the 2010 value) left to reduce. This means that for the coming years and decades, the influence on global warming rates from East Asian emissions reductions is likely to be less prominent, although this depends crucially on the still unresolved question of the linearity of aerosol–climate responses, in particular through aerosol–cloud interactions.

Methods

Simulations

This study uses Earth System Model simulations performed for the RAMIP²¹. RAMIP is part of the extended phase of the 6th Coordinated Model Intercomparison Project (CMIP6Plus), and builds on and extends historical (1850–2014) simulations delivered to CMIP6. The RAMIP baseline simulation is a Shared Socioeconomic Pathway with a weak air quality policy and consequently continued strong aerosol emissions (SSP3-7.0). In RAMIP perturbations, these emissions are exchanged for a strong air quality policy case (SSP1-2.6), for individual emission regions.

In this study, we use the RAMIP *East Asia* simulation (SSP370-eas126aer), where all anthropogenic aerosol emissions from a geographical box consisting mainly of China are perturbed. All participating models ran the baseline and signal simulations for the period 2015–2049 and delivered 10 ensemble members for each simulation. See Supplementary Table 1 for an overview of the simulations.

A subset of the models also delivered simulations with fixed sea-surface temperatures, which can be used to quantify the ERF. See ref. 21 for details.

As part of Fig. 1, we also show the aerosol emissions trajectories of the signal and baseline simulations. All non-aerosol emissions are identical in signal and baseline, and they each branch off from the same ensemble members from the historical simulation in 2014. Land use change is also identical in signal and baseline (SSP3-7.0).

Models

Supplementary Table 2 lists the eight models used for the present study, together with the spatial resolutions, aerosol representation, and main references.

Analysis

Climate responses are defined as the difference between SSP370 and SSP370-eas126aer, for the period 2035–2049. For statistical significance, we require that the multi-model, multi-ensemble member sets (consisting of 80 global or regional means, or grid point values) are significantly different according to a paired t-test with $p < 0.05$. Map figures are hatched for all grid points that show statistically significant changes.

ERF is quantified as the difference in net TOA (shortwave + longwave) radiation between 30-year fSST simulations, following Forster et al.⁴².

Uncertainties

All uncertainties quoted in this paper are ± 1 standard deviation, generally of the set of ensemble mean results from each model.

Regions

East Asia is here defined as a geographical box covering 20N–35N, 95E–133E.

Observational data

Additionally, we use gridded aerosol emissions data from CEDS (2024 Gridded Data Release: December 3, 2024; v_2024_11_25), observations of aerosol optical depths from the MODIS instruments on the Terra and Aqua satellites (Combined Dark Target and Deep Blue AOD at 0.55 micron; MYD08_M3 v6.1 and MOD08_M3 v6.1), TOA energy imbalance observations from the CERES instrument (EBAF-TOA_v4.2.1), and TOA energy imbalance estimates from the ERA5 reanalysis³⁵.

Data availability

Processed RAMIP datasets used in this paper are available from figshare archive <https://doi.org/10.6084/m9.figshare.28296344>⁴³. Other datasets are available as described in “Methods,” with full links to the simulation datasets shown in Supplementary Table 3.

Code availability

The analysis code used to produce the figures and key results is available from the figshare archive <https://doi.org/10.6084/m9.figshare.28296344>⁴³.

Received: 11 April 2025; Accepted: 27 June 2025;

Published online: 14 July 2025

References

- Merchant, C. J., Allan, R. P. & Embury, O. Quantifying the acceleration of multidecadal global sea surface warming driven by Earth’s energy imbalance. *Environ. Res. Lett.* **20**, <https://doi.org/10.1088/1748-9326/adaa8a> (2025).
- Forster, P. M. et al. Indicators of Global Climate Change 2023: annual update of key indicators of the state of the climate system and human influence. *Earth Syst. Sci. Data* **16**, 2625–2658 (2024).
- Samset, B. H. et al. Steady global surface warming from 1973 to 2022 but increased warming rate after 1990. *Commun. Earth Environ.* **4**, <https://doi.org/10.1038/s43247-023-01061-4> (2023).
- van der A, R. J. et al. Cleaning up the air: effectiveness of air quality policy for SO₂ and NO_x emissions in China. *Atmos. Chem. Phys.* **17**, 1775–1789 (2017).
- Zheng, Y., Zhang, Q., Tong, D., Davis, S. J. & Caldeira, K. Climate effects of China’s efforts to improve its air quality. *Environ. Res. Lett.* **15**, <https://doi.org/10.1088/1748-9326/ab9e21> (2020).
- IPCC. Summary for policymakers. In *Climate Change 2021: The Physical Science Basis. Contribution of Working Group I to the Sixth Assessment Report of the Intergovernmental Panel on Climate Change* (eds Masson-Delmotte, V. et al.) (Cambridge University Press, 2021).
- Forster, P. & Storelvmo, T. The Earth’s energy budget, climate feedbacks, and climate sensitivity. In *Working Group 1 contribution to the IPCC 6th Assessment Report* (eds Masson-Delmotte, V. et al.) Ch. 7 (Cambridge University Press, 2021).
- Samset, B. H., Lund, M. T., Bollasina, M., Myhre, G. & Wilcox, L. Emerging Asian aerosol patterns. *Nat. Geosci.* **12**, 582–584 (2019).
- Zheng, B. et al. Trends in China’s anthropogenic emissions since 2010 as the consequence of clean air actions. *Atmos. Chem. Phys.* **18**, 14095–14111 (2018).
- Samset, B. H., Lund, M. T., Fuglestad, J. S. & Wilcox, L. J. 2023 temperatures reflect steady global warming and internal sea surface temperature variability. *Commun. Earth Environ.* **5**, <https://doi.org/10.1038/s43247-024-01637-8> (2024).

11. Loeb, N. G. et al. Observational assessment of changes in Earth's energy imbalance since 2000. *Surv. Geophys.* <https://doi.org/10.1007/s10712-024-09838-8> (2024).
12. Hodnebrog, Ø. et al. Recent reductions in aerosol emissions have increased Earth's energy imbalance. *Commun. Earth Environ.* **5**, <https://doi.org/10.1038/s43247-024-01324-8> (2024).
13. Gettelman, A. et al. Has reducing ship emissions brought forward global warming? *Geophys. Res. Lett.* **51**, e2024GL109077 (2024).
14. Skeie, R. B., Byrom, R., Hodnebrog, Ø., Jouan, C. & Myhre, G. Multi-model effective radiative forcing of the 2020 sulfur cap for shipping. *Atmos. Chem. Phys.* **24**, 13361–13370 (2024).
15. Goessling, H. F., Rackow, T. & Jung, T. Recent global temperature surge intensified by record-low planetary albedo. *Science* **387**, 68–73 (2025).
16. Eyring, V. et al. Overview of the Coupled Model Intercomparison Project Phase 6 (CMIP6) experimental design and organization. *Geosci. Model Dev.* **9**, 1937–1958 (2016).
17. Szopa, S. et al. In *Climate Change 2021: The Physical Science Basis. Contribution of Working Group I to the Sixth Assessment Report of the Intergovernmental Panel on Climate Change* (eds Masson-Delmotte, V. et al.) 817–922 (Cambridge University Press, 2021).
18. Wang, Z. et al. Incorrect Asian aerosols affecting the attribution and projection of regional climate change in CMIP6 models. *npj Clim. Atmos. Sci.* **4**, <https://doi.org/10.1038/s41612-020-00159-2> (2021).
19. Wang, H. et al. Atmosphere teleconnections from abatement of China aerosol emissions exacerbate Northeast Pacific warm blob events. *Proc. Natl. Acad. Sci. USA* **121**, e2313797121 (2024).
20. Yao, N. et al. Less anthropogenic aerosol indirect effects are a potential cause for Northeast Pacific warm blob events. *Proc. Natl. Acad. Sci. USA* **121**, e2414614121 (2024).
21. Wilcox, L. J. et al. The Regional Aerosol Model Intercomparison Project (RAMIP). *Geosci. Model Dev.* **16**, 4451–4479 (2023).
22. Hoesly, R. M. et al. Historical (1750–2014) anthropogenic emissions of reactive gases and aerosols from the Community Emissions Data System (CEDS). *Geosci. Model Dev.* **11**, 369–408 (2018).
23. Samset, B. H. Aerosol absorption has an underappreciated role in historical precipitation change. *Commun. Earth Environ.* **3**, <https://doi.org/10.1038/s43247-022-00576-6> (2022).
24. Stjern, C. W. et al. The time scales of climate responses to carbon dioxide and aerosols. *J. Clim.* **36**, 3537–3551 (2023).
25. Graff, L. S. et al. Sensitivity of winter Arctic amplification in NorESM2. EGUSphere. <https://doi.org/10.5194/egusphere-2025-472> (2025).
26. Watson-Parris, D. et al. Weak surface temperature effects of recent reductions in shipping SO₂ emissions, with quantification confounded by internal variability. <https://doi.org/10.5194/egusphere-2024-1946> (2024).
27. Fadnavis, S. et al. Long range transport of South and East Asian anthropogenic aerosols counteracting Arctic warming. *npj Clim. Atmos. Sci.* **7**, <https://doi.org/10.1038/s41612-024-00633-1> (2024).
28. Stjern, C. W. et al. Rapid adjustments cause weak surface temperature response to increased black carbon concentrations. *J. Geophys. Res. Atmos.* **122**, 11,462–411,481 (2017).
29. Xiang, B., Xie, S.-P., Kang, S. M. & Kramer, R. J. An emerging Asian aerosol dipole pattern reshapes the Asian summer monsoon and exacerbates northern hemisphere warming. *npj Clim. Atmos. Sci.* **6**, <https://doi.org/10.1038/s41612-023-00400-8> (2023).
30. Wilcox, L. J. et al. Mechanisms for a remote response to Asian anthropogenic aerosol in boreal winter. *Atmos. Chem. Phys.* **19**, 9081–9095 (2019).
31. Samset, B. H. et al. Weak hydrological sensitivity to temperature change over land, independent of climate forcing. *npj Clim. Atmos. Sci.* **1**, <https://doi.org/10.1038/s41612-017-0005-5> (2018).
32. Allen, R. J., Evan, A. T. & Booth, B. B. Interhemispheric aerosol radiative forcing and tropical precipitation shifts during the late twentieth century. *J. Clim.* **28**, 8219–8246 (2015).
33. Myhre, G. et al. Multi-model simulations of aerosol and ozone radiative forcing due to anthropogenic emission changes during the period 1990–2015. *Atmos. Chem. Phys.* **17**, 2709–2720 (2017).
34. Ren, X., Liu, W., Capotondi, A., Amaya, D. J. & Holbrook, N. J. The Pacific Decadal Oscillation modulated marine heatwaves in the Northeast Pacific during past decades. *Commun. Earth Environ.* **4**, <https://doi.org/10.1038/s43247-023-00863-w> (2023).
35. Hersbach, H. et al. The ERA5 global reanalysis. *Q. J. R. Meteorol. Soc.* **146**, 1999–2049 (2020).
36. Lan, X., Thoning, K. W. & Dlugokencky, E. J. Trends in globally-averaged CH₄, N₂O, and SF₆ determined from NOAA Global Monitoring Laboratory measurements. Version 2025-03, <https://doi.org/10.15138/P8XG-AA10> (2022).
37. Gulev, S. K. et al. in *Climate Change 2021: The Physical Science Basis. Contribution of Working Group I to the Sixth Assessment Report of the Intergovernmental Panel on Climate Change* (eds Masson-Delmotte, V. et al.) 287–422 (Cambridge University Press, 2021).
38. Etminan, M., Myhre, G., Highwood, E. J. & Shine, K. P. Radiative forcing of carbon dioxide, methane, and nitrous oxide: A significant revision of the methane radiative forcing. *Geophys. Res. Lett.* **43**, 12,614–12,623 (2016).
39. Allen, R. J. et al. Surface warming and wetting due to methane's long-wave radiative effects muted by short-wave absorption. *Nat. Geosci.* **16**, 314–320 (2023).
40. Quaglia, I. & Visioni, D. Modeling 2020 regulatory changes in international shipping emissions helps explain anomalous 2023 warming. *Earth Syst. Dyn.* **15**, 1527–1541 (2024).
41. Yuan, T. et al. Abrupt reduction in shipping emission as an inadvertent geoengineering termination shock produces substantial radiative warming. *Commun. Earth Environ.* **5**, 281 (2024).
42. Forster, P. M. et al. Recommendations for diagnosing effective radiative forcing from climate models for CMIP6. *J. Geophys. Res. Atmos.* <https://doi.org/10.1002/2016JD025320> (2016).
43. Samset, B. H. et al. <https://doi.org/10.6084/m9.figshare.28296344> (Figshare, 2025).

Acknowledgements

We acknowledge support by the Center for Advanced Study in Oslo, Norway which funded and hosted the HETCLIF center during the academic year of 2023/24. The NorESM simulations were enabled by resources provided by the National Academic Infrastructure for Supercomputing in Sweden (NAISS). We also acknowledge the following funding sources: Research Council of Norway grant 324182 (CATHY; B.H.S., L.J.W., C.W.S., M.T.L., R.J.A.). Horizon Europe grant 101137639 (CleanCloud; B.H.S., M.T.L., L.J.W.). National Science Foundation grant #AGS-2153486 (R.J.A.). Natural Environment Research Council (NERC) grant TerraFIRMA NE/W004895/1 (L.J.W., P.T.G., S.T.R.). National Center for Atmospheric Science, UK (L.J.W., S.T.R.). Environment Research and Technology Development Fund (JPMEERF20232001) of the Environmental Restoration and Conservation Agency was provided by the Ministry of the Environment of Japan (T.K., N.O.). Arctic Challenge for Sustainability II (ArCS II), Program Grant Number JPMXD1420318865 (TK, NO). Global Environmental Research Coordination System from the Ministry of the Environment of Japan grant MLIT2253 (T.K., N.O.). H2020 Societal Challenges grant no. 101003826 (J.M., R.M., D.O.D.). Research Council Finland grant no. 337552 (J.M., R.M., D.O.D.). Columbia Center for Climate and Life (D.M.W.). Natural Sciences and Engineering Research Council of Canada (NSERC) (P.K., L.F.L.). Swedish Research Council through grant agreement no. 2022-06725 (A.L.).

Author contributions

B.H.S. and L.J.W. conceived the study. B.H.S., L.J.W., C.W.S., R.J.A., and M.T.L. performed the analysis and wrote the paper. P.K., L.F.L., R.A.,

D.M.W., A.E., K.T., T.T., J.M., D.O., R.M., A.L., L.W., S.R., J.K., P.G., N.O., T.K., P.N., and L.N. designed and/or delivered simulations. L.J.W., S.A., and M.T.E. performed dataset preparations. All authors contributed to editing and finalizing the paper.

Competing interests

The authors declare no competing interests.

Additional information

Supplementary information The online version contains supplementary material available at <https://doi.org/10.1038/s43247-025-02527-3>.

Correspondence and requests for materials should be addressed to Bjørn H. Samset.

Peer review information *Communications Earth and Environment* thanks Velle Toll and the other, anonymous, reviewer(s) for their contribution to the peer review of this work. Primary Handling Editor: Alice Drinkwater. A peer review file is available.

Reprints and permissions information is available at <http://www.nature.com/reprints>

Publisher's note Springer Nature remains neutral with regard to jurisdictional claims in published maps and institutional affiliations.

Open Access This article is licensed under a Creative Commons Attribution 4.0 International License, which permits use, sharing, adaptation, distribution and reproduction in any medium or format, as long as you give appropriate credit to the original author(s) and the source, provide a link to the Creative Commons licence, and indicate if changes were made. The images or other third party material in this article are included in the article's Creative Commons licence, unless indicated otherwise in a credit line to the material. If material is not included in the article's Creative Commons licence and your intended use is not permitted by statutory regulation or exceeds the permitted use, you will need to obtain permission directly from the copyright holder. To view a copy of this licence, visit <http://creativecommons.org/licenses/by/4.0/>.

© The Author(s) 2025